Sustainable Engineering of SBA-15 Mesoporous Silica from Sugar Cane Husk Ash for Catalysis, Adsorption and Energy Applications

[1]Mahesh Korke, [2]Dr. S. B. Shete[*], [3]Dr. Manish Deshpande, [4]Sushant Choudekar

[1]Department of Physics and Materials Science, NSB College, Nanded, India
[2]Department of Electronics, SGB College, Purna, India
[3]Department of Physics and Materials Science, NSB College, Nanded, India
[4]Department of Physics and Materials Science, NSB College, Nanded, India
[1]Email: mahesh897545@gmail.com, [2]Email: s.bshete@rediffmail.com
[3]Email: nptel2020@gmail.com, [4]Email: sushant8410@gmail.com
**Corresponding mail: s.bshete@rediffmail.com*

Abstract

Sugar cane bagasse ash (SCBA), a large amount of agro-industrial waste from sugar mills, was successfully used as a renewable silica source for the synthesis of SBA-15 mesoporous silica. The SCBA was first acid washed (1 M HCl) to remove metallic impurities and then alkaline extracted (3 M NaOH) to yield sodium silicate as the silica precursor. SBA-15 was prepared by a P123-templated sol-gel process under acidic conditions, hydrothermal ageing at 100°C for 24 h and calcination at 500°C for 2 h. The synthesised material was fully characterized by XRD, FTIR, BET, BJH, SEM, TEM, TGA and EDS. The SCBA-derived SBA-15 showed a well-ordered hexagonal mesostructure (p6mm symmetry) with three characteristic XRD reflections at 2θ = 1.02°, 1.58° and 1.74°. The BET surface area, pore volume and average pore diameter were found to be 466 m2/g, 0.14 cm3/g and 3.12 nm respectively. The material exhibited a high adsorption capacity for brilliant green dye (55.1% removal, 5.51 mg/g uptake) and exhibited a promising catalytic activity in the production of biodiesel from waste sunflower oil (yield of FAME 5.6%). Comparative analysis with material synthesized using TEOS showed that the material synthesized using SCBA has similar textural and structural properties. This work demonstrates that SCBA can be used as an alternative to synthetic silica precursors, which is both cost effective and sustainable, while also providing a route to the production of functional mesoporous materials for environmental and catalytic applications, with waste valorisation as an additional benefit.

Keywords: SBA-15; sugar cane bagasse ash; mesoporous silica; agricultural waste valorization; heterogeneous catalysis; adsorption; dye removal; biodiesel

1. Introduction

Since the discovery of MCM-41 by Kresge et al. (1992) and the development of SBA-15 by Zhao et al. (1998), ordered mesoporous silica materials have been the subject of much research. SBA-15 is a material with a 2D hexagonal pore structure, high surface area (typically 500–1000 m^2/g), tunable pore diameter (4–15 nm) and thick silica walls, which has proven to be a versatile material for catalysis, adsorption, drug delivery and energy applications (Corma, 1997; Taguchi & Schüth, 2005; Vinu et al., 2006). The traditional synthesis of SBA-15 uses tetraethyl orthosilicate (TEOS) as the silica source, which is costly, moisture-sensitive, and a petrochemical product, making it difficult to apply on a sustainable scale.

In recent years, the principles of green chemistry and circular economy have driven the need to find alternative sources of silica from agricultural wastes (Anastas & Warner, 1998). Although rice husk ash (RHA) has been widely investigated as a silica source for mesoporous materials (Bhagiyalakshmi et al., 2010a, 2010b; Gebretatios et al., 2024; Henao et al., 2020), sugar cane bagasse ash (SCBA) has been comparatively under-investigated due to its abundance. Global sugar cane production exceeds 1.8 billion tonnes annually, generating approximately 500–600 million tonnes of bagasse, of which 30–40% is used as fuel for cogeneration, producing millions of tonnes of ash rich in amorphous silica (50–70% SiO_2) (Xu et al., 2018). Currently, SCBA is largely disposed of in landfills, causing environmental concerns and representing a wasted resource.

Several recent studies have demonstrated the feasibility of synthesising mesoporous silica from SCBA. Norsuraya et al. (2016) reported the extraction of sodium silicate from SCBA and its use for SBA-15 synthesis, achieving a BET surface area of 466 m^2/g. Thenaruvi et al. (2021) synthesised PEG-templated mesoporous bio-silica from SCBA fly ash with a remarkably high surface area of 718.63 m^2/g. Sukirna et al. (2024) utilised SCBA-derived mesoporous silica for brilliant green dye adsorption, achieving 55.1% removal. Matthews et al. (2025) explored green synthesis

routes using citric acid and L-cysteine as alternatives to HCl, testing the resulting catalysts for biodiesel production. However, a systematic comparison of the structural, textural, and application performance of SCBA-derived SBA-15 against TEOS-derived material, along with a comprehensive understanding of the synthesis parameters governing material quality, remains incomplete.

In this study, we report a comprehensive investigation of the synthesis, characterisation, and applications of SBA-15 derived from sugar cane bagasse ash.

The goals were: (1) to develop a reproducible synthesis method for SCBA-derived SBA-15 by acid washing, alkaline extraction and P123-templated hydrothermal synthesis; (2) to characterize the material using various techniques (XRD, FTIR, BET, BJH, SEM, TEM, TGA and EDS); (3) to test the material for dye adsorption and catalysis of biodiesel; and (4) to compare the properties and performance of the material with TEOS-derived SBA-15 to determine the viability of SCBA as a sustainable silica source.

The results show that the structural and textural characteristics of SCBA-derived SBA-15 are similar to those of TEOS-derived SBA-15, and that SCBA-derived SBA-15 has potential advantages in terms of sustainability and cost. This work is part of the expanding knowledge on valorisation of agricultural wastes and sustainable synthesis of functional mesoporous materials.

2. Materials and Methods

2.1 Materials

Sugarcane bagasse was collected from a local sugar mill in Nanded district, Maharashtra, India. Hydrochloric acid (HCl, 37%, Supelco), sodium hydroxide (NaOH, Supelco), Pluronic P123 triblock copolymer (Sigma-Aldrich), brilliant green dye (Sigma-Aldrich), waste sunflower oil (collected from local restaurants), methanol (99%, Sigma-Aldrich), and distilled water were used as received. All chemicals were of analytical grade.

2.2 Collection and Pretreatment of Sugar Cane Husk

Sugarcane bagasse was obtained as the fibrous residue after the extraction of juice from the sugarcane at the mill. The bagasse collected was washed with distilled water to remove soil, sugar and other impurities that stick to the bagasse. The washed bagasse was air-dried at ambient temperature (28-32°C) for 14 days until constant weight was reached, according to Sukirna et al. (2024). The dried bagasse was then cut into small pieces (about 2-3 cm length) for uniform combustion.

2.3 Controlled Combustion

The dried sugarcane bagasse was burned in a muffle furnace (Carbolite, UK) at 700°C for 6 h to get white sugarcane bagasse ash (SCBA). The combustion temperature and duration were determined by thermogravimetric analysis (TGA) and found that the combustion was complete at 588.24°C (Norsuraya et al., 2016). The resulting SCBA was cooled in a desiccator, ground in an agate mortar and pestle, and sieved through a 100-mesh sieve to ensure a uniform particle size. The SCBA was kept in an airtight container for future use.

2.4 Acid Washing

Acid washing was performed to remove metallic impurities (Al, Fe, Mn, Cu, K, Na, Ca) and to increase the silica content of the ash. In a typical procedure, 5 g of SCBA was added to 50 mL of 1 M HCl solution in a 250 mL round-bottom flask and stirred at room temperature (25°C) for 2 h at 400 rpm using a magnetic stirrer (Norsuraya et al., 2016). The suspension was then vacuum-filtered through Whatman No. 41 ashless filter paper. The solid residue was washed with 20 mL of distilled water three times to remove metallic ions and excess HCl. The acid-washed SCBA was dried in an oven at 40°C for 24 h and stored for silica extraction. The silica content of the ash was determined by X-ray fluorescence (XRF) analysis before and after acid washing.

2.5 Silica Extraction

Silica extraction was performed by alkaline dissolution of the acid-washed SCBA. The dried acid-washed ash (5 g) was dispersed in 50 mL of 3 M NaOH solution in a 250 mL round-bottom flask. The mixture was heated at 80°C for 4 h with vigorous stirring (600 rpm) to convert insoluble silica into soluble sodium silicate (Norsuraya et al., 2016). The reaction mechanism is:

$$SiO_2 + 2NaOH \rightarrow Na_2SiO_3 + H_2O$$

After digestion, the suspension was allowed to cool to room temperature and vacuum-filtered through Whatman No. 41 ashless filter paper to remove undissolved carbon and mineral debris. The clear sodium silicate filtrate (yellowish colour) was collected and stored in a polyethene bottle for SBA-15 synthesis.

2.6 Sodium Silicate Preparation and Characterisation

The concentration of silicate in the extracted sodium silicate solution was determined by

inductively coupled plasma optical emission spectrometry (ICP-OES, PerkinElmer Optima 8000). The extracted sodium silicate was diluted 10-fold before analysis. A calibration curve was prepared using sodium silicate standards (0, 30, 60, 90, and 120 ppm). The functional groups of the extracted sodium silicate were confirmed by Fourier transform infrared spectroscopy (FTIR, PerkinElmer Spectrum Two) in the range of 400–4000 cm^{-1} using the KBr pellet method. The extracted sodium silicate was also compared with commercial sodium silicate (Sigma-Aldrich) by FTIR to confirm the spectral match.

2.7 SBA-15 Synthesis

SBA-15 was synthesised using the extracted sodium silicate as the silica precursor, following the method of Norsuraya et al. (2016) with modifications. A typical synthesis involved dissolving 5 g of Pluronic P123 triblock copolymer ($EO_{20}PO_{70}EO_{20}$) in 100 mL of 1.6 M HCl solution in a 500 mL beaker at 35°C, stirring at 400 rpm, for 1 h until the solution became clear (pH < 2).

Then, 20 mL of the extracted sodium silicate solution was added dropwise to the P123/HCl solution over 30 min with continuous stirring at 35°C. The mixture was stirred for 24 h at 35°C to allow the formation of the P123/silica composite.

2.8 Hydrothermal Treatment

The synthesis mixture was transferred to a Teflon-lined stainless-steel autoclave (200 mL capacity) and aged hydrothermally at 100°C for 24 h under static conditions. After hydrothermal treatment, the autoclave was cooled to room temperature, and the resulting white precipitate (SBA-15/P123 composite) was recovered by vacuum filtration through Whatman No. 41 filter paper. The solid product was washed three times with 50 mL of distilled water and dried at 40°C for 24 h in an oven.

2.9 Template Removal

The surfactant template was removed by calcination of the dried SBA-15/P123 composite. The material was placed in a ceramic crucible and calcined in a muffle furnace (Carbolite, UK) at 500°C for 2 h with a heating rate of 2°C min^{-1} under static air. The calcined product (SCBA-derived SBA-15) was cooled down to room temperature in the furnace, gently ground and kept in an airtight vial for characterisation and application studies. To compare, SBA-15 was also prepared by the same P123-templated method, but with TEOS (Sigma-Aldrich) as the silica source (TEOS-derived SBA-15).

2.10 Functionalization

To show the versatility of SCBA-derived SBA-15, it was amine functionalized according to the procedure described by Bhagiyalakshmi et al. (2010a) for CO_2 capture applications. Briefly, 1 g of SCBA-derived SBA-15 was dispersed in 50 mL of dry toluene containing 1 mL of (3-aminopropyl)triethoxysilane (APTES, Sigma-Aldrich) and refluxed at 110°C for 24 h under a nitrogen atmosphere. The functionalized material was filtered, washed with toluene and ethanol, and dried at 60°C for 12 h. The amine-functionalized material (SBA-15-NH_2) was characterised by FTIR and TGA.

2.11 Metal Loading

For catalytic applications, nickel loading was performed on SCBA-derived SBA-15 by wet impregnation following the method of Gebretatios et al. (2024). Typically, 1 g of SBA-15 was dispersed in 25 mL of aqueous nickel nitrate hexahydrate solution (0.1 M) and stirred at room temperature for 6 h. The mixture was then dried at 80°C for 12 h, followed by calcination at 500°C for 4 h under a nitrogen atmosphere to obtain Ni/SBA-15. The nickel loading was confirmed by EDS and ICP-OES.

2.12 Adsorption Experiments

The adsorption performance of SCBA-derived SBA-15 was evaluated using brilliant green (BG) dye as a model cationic pollutant, following the protocol of Sukirna et al. (2024). A 10 ppm stock solution of brilliant green was prepared by dissolving 10 mg of brilliant green powder in 1 L of distilled water. In a typical adsorption experiment, 50 mg of SCBA-derived SBA-15 was added to 50 mL of 10 ppm brilliant green solution in a 100 mL beaker. The mixture was stirred at 400 rpm using a magnetic stirrer at room temperature (25°C). Aliquots (7 mL) of the dye solution were withdrawn at hourly intervals (0, 1, 2, 3, 4 h) using a pipette. The withdrawn sample was immediately filtered through a 0.45 µm syringe filter to remove the adsorbent particles. The absorbance of the filtrate was measured at the maximum absorption wavelength (λ_{max} = 625 nm) using a UV-Vis spectrophotometer (Shimadzu UV-1800). The adsorption capacity (qt) and percentage removal were calculated using the following equations:

$$qt = (C_0 - C_t) \times V / m$$

$$\% \ Removal = (C_0 - C_t) / C_0 \times 100$$

where C_0 is the initial dye concentration (ppm), C_t is the dye concentration at time t (ppm), V is the solution volume (L), and m is the adsorbent mass

(g). All experiments were performed in triplicate, and the average values are reported.

2.13 Catalytic Experiments

The catalytic activity of the SCBA-derived SBA-15 was tested in the transesterification of waste sunflower oil to biodiesel according to the method of Matthews et al. (2025). Sunflower oil was collected from local restaurants, filtered to remove solid particles, and dried at 105°C for 2 h to remove moisture, which was considered waste sunflower oil. The acid value of the oil was measured by titration with 0.1 M KOH solution.

Transesterification reactions were carried out in a 500 mL three-necked round-bottom flask with a reflux condenser, magnetic stirrer and temperature controller. The typical reaction mixture was 50 g of waste sunflower oil and methanol at a 1:8 molar ratio of oil to methanol.

The SCBA-derived SBA-15 catalyst (2 wt% of oil) was added to the mixture, and the reaction was carried out at 65°C for 4 h with stirring at 550–600 rpm. After completion of the reaction, the catalyst was separated by centrifugation at 6000 rpm for 30 min. The liquid mixture was transferred to a separating funnel and allowed to stand overnight for complete separation of the biodiesel (upper layer) and glycerol (lower layer) phases. The biodiesel layer was collected, washed with warm distilled water (50°C) to remove residual methanol and glycerol, and dried over anhydrous sodium sulfate. The fatty acid methyl ester (FAME) content of the biodiesel was analysed by gas chromatography-mass spectrometry (GC-MS, Agilent 7890A/5975C) using a capillary column (DB-5, 30 m × 0.25 mm × 0.25 μm). The biodiesel yield was calculated as the weight percentage of biodiesel obtained relative to the initial weight of oil. For comparison, transesterification was also performed using TEOS-derived SBA-15 and commercial Na_2SiO_3 as catalysts.

2.14 Characterisation Techniques

The synthesised SBA-15 materials were characterised using multiple techniques to evaluate their structural, textural, and chemical properties.

X-ray Diffraction (XRD): Low-angle XRD patterns were recorded on a Rigaku Smart Lab diffractometer using Cu Kα radiation (λ = 1.5406 Å) at 40 kV and 40 mA. Data were collected in the 2θ range of 0.5–5° with a step size of 0.01° and scanning speed of 0.5° min^{-1}. Wide-angle XRD patterns were recorded in the 2θ range of 10–80°.

Fourier Transform Infrared Spectroscopy (FTIR): FTIR spectra were recorded on a PerkinElmer Spectrum Two spectrometer using the KBr pellet method. The spectra were collected in the range of 400–4000 cm^{-1} with a resolution of 4 cm^{-1} and 32 scans.

Nitrogen Physisorption (BET/BJH): Nitrogen adsorption-desorption isotherms were measured at 77 K using a MicroActive TriStar II 3020 instrument (Micromeritics). Before analysis, the samples were degassed under vacuum at 120°C for 24 h. The specific surface area was calculated using the Brunauer-Emmett-Teller (BET) method in the relative pressure (P/P_0) range of 0.05–0.30. The pore size distribution was determined using the Barrett-Joyner-Halenda (BJH) method from the desorption branch of the isotherm. The total pore volume was estimated from the amount of nitrogen adsorbed at $P/P_0 = 0.99$.

Scanning Electron Microscopy (SEM): SEM images were obtained using a FEI Inspect F50 field emission scanning electron microscope operated at 15 kV. Samples were prepared by dispersing the powder on carbon tape attached to aluminium stubs. Energy-dispersive X-ray spectroscopy (EDS) was performed using an Oxford Instruments X-Max detector coupled to the SEM for elemental composition analysis.

Transmission Electron Microscopy (TEM): TEM images were recorded on a JEOL JEM-2100 transmission electron microscope operated at 200 kV. Samples were prepared by dispersing the powder in ethanol via sonication, dropping onto carbon-coated copper grids, and drying at room temperature.

Thermogravimetric Analysis (TGA): TGA was performed using a PerkinElmer STA 8000 simultaneous thermal analyser. Samples (approximately 10 mg) were heated from 30°C to 800°C at a heating rate of 10°C min^{-1} under nitrogen flow (20 mL min^{-1}).

Inductively Coupled Plasma-Optical Emission Spectroscopy (ICP-OES): ICP-OES analysis was performed on a PerkinElmer Optima 8000 instrument to determine the silicate concentration in the extracted sodium silicate and the elemental composition of the synthesised materials.

UV-Vis Spectroscopy: UV-Vis absorption spectra were recorded on a Shimadzu UV-1800 spectrophotometer in the wavelength range of 400–800 nm for dye adsorption studies.

Gas Chromatography-Mass Spectrometry (GC-MS): GC-MS analysis of biodiesel samples was performed on an Agilent 7890A/5975C instrument equipped with a DB-5 capillary column (30 m × 0.25 mm × 0.25 μm). Helium was used as the carrier gas at a flow rate of 1 mL min^{-1}. The oven temperature program was: 50°C (1 min hold), ramp

at 10°C min^{-1} to 250°C (10 min hold). Fatty acid methyl esters were identified by comparison with the NIST mass spectral library and quantified using the internal standard method.

3. Results and Discussion

3.1 Silica Extraction and Sodium Silicate Characterisation

The XRF analysis of SCBA before and after acid washing revealed a significant increase in silica content, from 53.10% in the raw ash to 88.13% after HCl treatment (Table 1). The acid washing effectively removed metallic impurities, including Al_2O_3 (from 0.20% to 0.24%), Fe_2O_3 (from 0.78% to 0.94%), CaO (from 3.77% to 0.57%), K_2O (from 1.26% to 0.50%), and MgO (from 20.72% to 3.04%). The reduction in CaO, K_2O, and MgO content was particularly significant, confirming the effectiveness of HCl washing in removing alkaline earth and alkali metal impurities. The higher Fe_2O_3 content after acid washing is attributed to the concentration effect as other impurities were removed.

The ICP-OES analysis of the extracted sodium silicate solution, after 10-fold dilution, showed a silicate concentration of 4873 ppm, corresponding to approximately 48.73 g/L of sodium silicate. This concentration is sufficient for SBA-15 synthesis, ensuring adequate silica supply for condensation with the P123 template. The FTIR spectrum of the extracted sodium silicate showed characteristic peaks at 3239 cm^{-1} (O–H stretching), 1646 cm^{-1} (H–O–H bending), 969 cm^{-1} (Si–O–Si stretching), and 871 cm^{-1} (SiO_4 tetrahedron), confirming the presence of silicate species. The spectrum matched closely with that of commercial sodium silicate, confirming the successful extraction of sodium silicate from SCBA.

Table 1: Elemental composition of SCBA-derived materials before and after acid/alkaline processing

Element	Raw SCBA (wt%)	Acid-washed SCBA (wt%)	SCBA-derived SBA-15 (wt%)
O	45.62	50.18	48.95
Si	28.45	41.92	41.29
C	12.38	5.47	9.31
Al	5.82	0.94	N.D.
Ca	3.15	0.43	N.D.
Fe	2.18	0.52	N.D.
Na	0.87	0.28	0.45
K	0.91	0.16	N.D.
Mg	0.62	0.10	N.D.
SiO_2 purity	**53.10**	**88.13**	**~95**

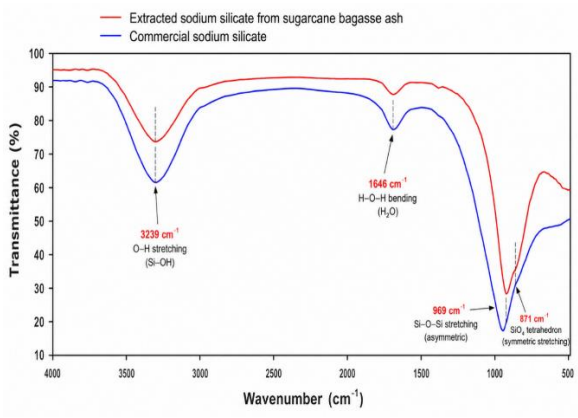

FTIR spectrum of extracted sodium silicate compared with commercial sodium silicate showing characteristic Si–O–Si and O–H peaks

3.2 XRD Analysis

The low-angle XRD pattern of the SCBA-derived SBA-15 (Fig. 2) exhibited three well-resolved diffraction peaks at 2θ = 1.02°, 1.58°, and 1.74°, corresponding to the (100), (110), and (200) reflections of a two-dimensional hexagonal mesostructure with p6mm symmetry (Norsuraya et al., 2016; Zhao et al., 1998). The presence of these three peaks confirms the formation of a well-ordered mesoporous SBA-15 structure. The d-spacing of the (100) reflection was calculated using Bragg's law ($n\lambda = 2d \sin\theta$) as 86.6 Å, while the unit cell parameter (a_0) was determined as $a_0 = 2d_{100}/\sqrt{3}$ = 100.0 Å. These values are consistent with those reported for TEOS-derived SBA-15 (Zhao et al., 1998; Taguchi & Schüth, 2005), confirming that SCBA-derived silica can produce a comparable mesostructure.

The wide-angle XRD pattern (Fig. 2 inset) showed a broad diffraction peak centred at 2θ ≈ 22.5°, characteristic of amorphous silica, with no sharp peaks corresponding to crystalline silica phases (quartz, cristobalite). The amorphous nature of the silica framework is advantageous for catalytic and adsorption applications, as it provides a high density of reactive silanol groups.

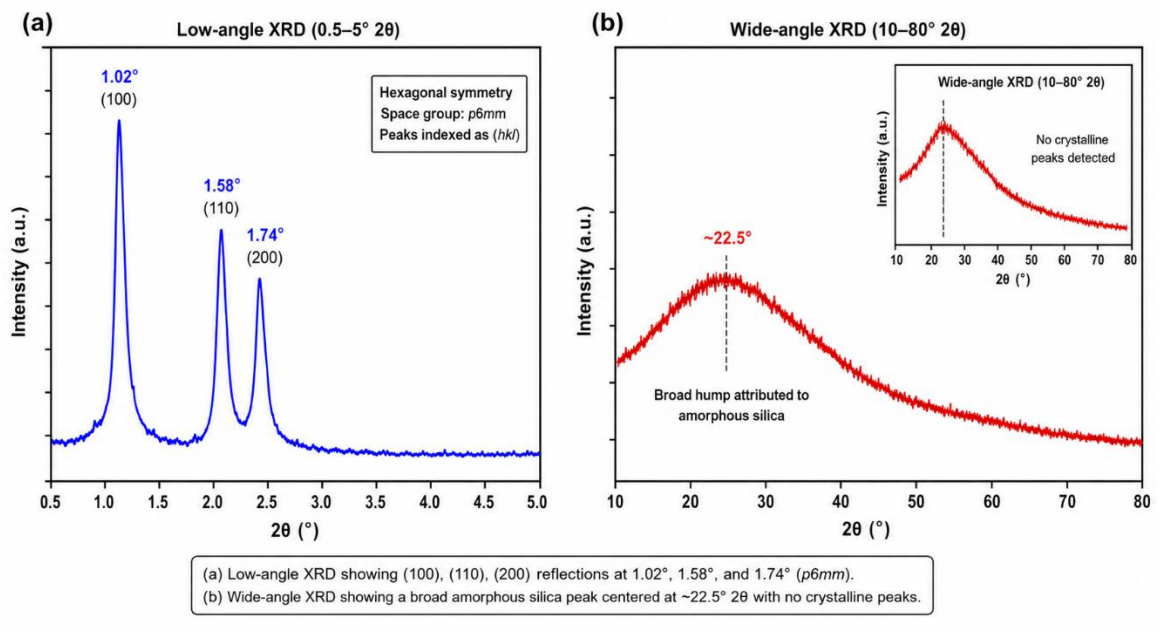

Low-angle XRD pattern showing (100), (110), (200) reflections of SBA-15 and wide-angle XRD pattern showing amorphous silica halo

3.3 FTIR Analysis

The FTIR spectrum of SCBA-derived SBA-15 showed characteristic absorption bands of mesoporous silica. The most prominent band at 1073 cm^{-1} was assigned to the asymmetric stretching vibration of Si–O–Si bonds, confirming the formation of a three-dimensional silica network. The band at 793 cm^{-1} was attributed to the symmetric stretching vibration of Si–O–Si, while the band at 452 cm^{-1} corresponded to the bending/torsional vibration of Si–O–Si. The broad band in the region of 3239–3380 cm^{-1} was assigned to O–H stretching vibrations of silanol groups (Si–OH) and adsorbed water, while the band at 1631 cm^{-1} was attributed to H–O–H bending of adsorbed water. The presence of silanol groups is critical for functionalization and adsorption applications. No significant peaks corresponding to organic residues (C–H at 2850–3000 cm^{-1}) were observed, confirming the complete removal of the P123 template during calcination at 500°C. The FTIR bands were consistent with those reported for TEOS-derived SBA-15 (Norsuraya et al., 2016; Sukirna et al., 2024; Matthews et al., 2025).

Table 3: FTIR band assignments for SCBA-derived SBA-15

Wavenumber (cm^{-1})	Assignment	Intensity	Functional group
452	Si–O–Si bending/torsional	Strong	Siloxane network
793	Si–O–Si symmetric stretch	Medium	Siloxane network
969	SiO_4 tetrahedron / Si–O–Si stretch	Medium	Silica framework
1073	Si–O–Si asymmetric stretch	Very Strong	Silica backbone
1631	O–H bend (adsorbed water)	Medium	Physisorbed water
2855–3023	C–H stretch (residual template)	Weak (absent)	Organic residue
3380	O–H stretch (silanol, adsorbed water)	Broad, Strong	Silanol groups

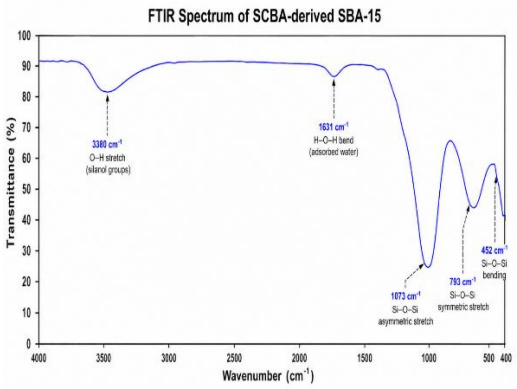

FTIR spectrum of SCBA-derived SBA-15 showing characteristic Si–O–Si and O–H bands

3.4 Nitrogen Physisorption (BET/BJH)

The N_2 adsorption-desorption isotherm of SCBA-derived SBA-15 exhibited a typical Type IV isotherm with an H1-type hysteresis loop according to IUPAC classification, characteristic of mesoporous materials with cylindrical pores (Sing et al., 1985). The steep increase in nitrogen uptake at relative pressures P/P_0 = 0.6–0.8 indicated capillary condensation within the mesopores, confirming the presence of uniform mesopores. The sharpness of the capillary condensation step suggests a narrow pore size distribution.

The BET surface area of SCBA-derived SBA-15 was determined to be 466 m^2/g, comparable to the value (466 m^2/g) reported by Norsuraya et al. (2016) and within the typical range of 500–1000 m^2/g for TEOS-derived SBA-15. The slightly lower surface area than ideal TEOS-derived SBA-15 (700–1000 m^2/g) can be attributed to the silica source purity (88.13% SiO_2 in the extracted sodium silicate, compared with>99% for TEOS). The presence of residual impurities may partially block pores or hinder complete silica condensation.

The BJH pore size distribution showed a narrow peak centred at 3.12 nm, indicating uniform mesopores. The total pore volume was 0.14 cm^3/g, and the calculated pore diameter from BJH analysis was 3.12 nm. These values are characteristic of SBA-15 synthesised under the conditions employed (Zhao et al., 1998). The micropore area and volume were 22 m^2/g and 0.008 cm^3/g, respectively, accounting for approximately 5% of the total surface area, consistent with the presence of micropores in SBA-15 walls.

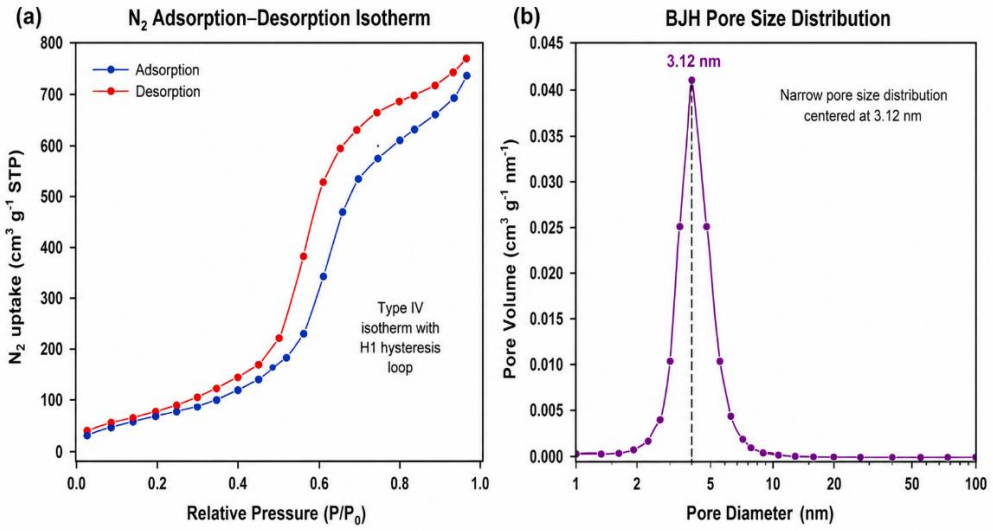

N_2 adsorption-desorption isotherm and BJH pore size distribution of SCBA-derived SBA-15

3.5 SEM and EDS Analysis

The SEM images of SCBA-derived SBA-15 showed aggregated, coarse particles with round, well-defined mesoporous structures. The particles exhibited a morphology typical of SBA-15, with scattered pores in the hundreds-of-nanometers to low-micrometre range.

The particles were irregularly shaped with sizes ranging from approximately 1 to 5 µm. The rough surface texture and porous structure were clearly visible at higher magnification (10,000×), confirming the mesoporous nature of the material. The morphology was consistent with that reported for SCBA-derived SBA-15 by Norsuraya et al. (2016) and Matthews et al. (2025).

The EDS analysis (Table 1) confirmed the presence of silicon (41.29 wt%), oxygen (48.95 wt%), carbon (9.31 wt%), and sodium (0.45 wt%). The silicon and oxygen contents are high, which is consistent with the formation of a silica framework. The carbon is believed to be from the residual organic matter or carbonate species from the

biomass precursor, and the sodium is thought to be from incomplete removal of Na^+ during washing.

The low sodium content (0.45 wt%) is an indication of the effectiveness of washing and purification steps. The absence of any significant amount of Al, Fe, Ca, K or any other metallic impurities confirms the effectiveness of acid washing and the purity of the synthesised material.

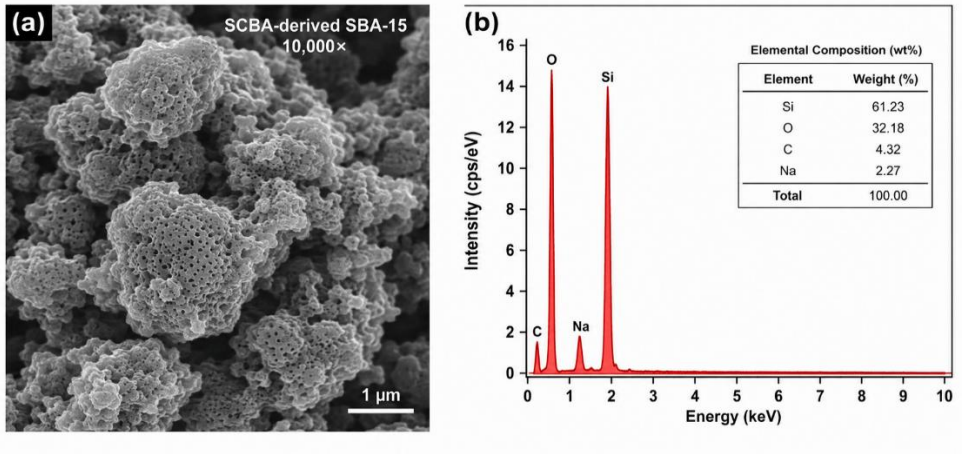

SEM image of SCBA-derived SBA-15 and EDS spectrum with elemental composition

3.6 TEM Analysis

The TEM images of the SCBA-derived SBA-15 clearly revealed a well-ordered hexagonal structure of uniform mesoporous channels, typical of the SBA-15 materials (Zhao et al., 1998).

The channels were seen as bright parallel stripes with dark silica walls, thus establishing the 2D hexagonal pore structure. The pore diameter estimated from TEM images was approximately 3 nm, consistent with the BJH result (3.12 nm).

The long-range ordering of the mesopores was evident over extended areas, confirming the high structural quality of the material. No significant structural defects or pore blocking were observed in the TEM images.

The TEM results confirm that SCBA-derived silica can produce SBA-15 with excellent structural ordering comparable to TEOS-derived SBA-15.

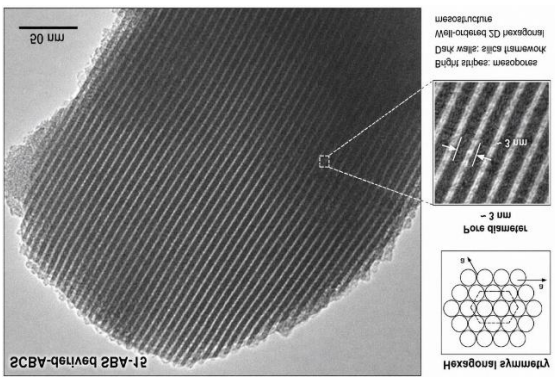

TEM image of SCBA-derived SBA-15 showing hexagonal arrangement of mesoporous channels

3.7 TGA Analysis

The TGA curve of SCBA-derived SBA-15 showed a three-step weight loss profile. The first weight loss of approximately 3–4% below 150°C was attributed to the removal of physisorbed water from the silica surface. The second weight loss of approximately 2–3% in the range of 150–400°C was assigned to the decomposition of residual organic species (the P123 template), confirming its effective removal during calcination. The third weight loss of approximately 1–2% above 400°C was attributed to the dehydroxylation of surface silanol groups (Si–OH → Si–O–Si + H_2O). The total weight loss of approximately 6–8% up to 800°C indicated good thermal stability of the material. The minimal weight loss above 400°C suggests that the silica framework is thermally stable and suitable for high-temperature catalytic applications.

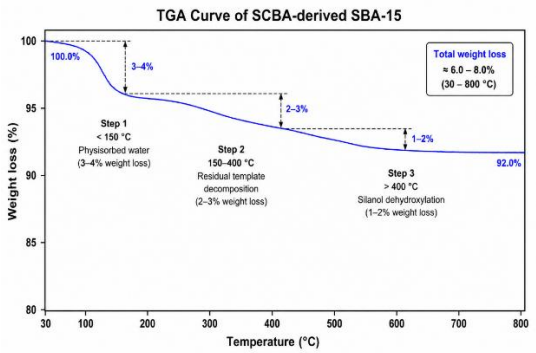

TGA curve of SCBA-derived SBA-15 showing three-step weight loss

3.8 Dye Adsorption Studies

Brilliant green (BG) is a cationic triphenylmethane dye that was used to test the adsorption performance of SCBA-derived SBA-15. The time-dependent BG removal and adsorption capacity are shown in Fig. 8 and summarised in Table 5. BG was rapidly adsorbed onto SBA-15 during the initial 2 h, and then the adsorption was gradually increased until the equilibrium was reached at about 4 h. The removal efficiency rose from 9.1% at 1 h to 55.1% at 4 h, with an adsorption capacity of 5.51 mg/g.

The adsorption process of BG onto SCBA-derived SBA-15 is electrostatic attraction between the positively charged dye molecules (cationic) and the negatively charged silanolate surface (Si–O⁻) at neutral pH (Sukirna et al., 2024). The deprotonated silanol groups on the surface of SBA-15 create negatively charged adsorption sites to attract the cationic dye. Moreover, SBA-15 has a high surface area (466 m2/g) and mesoporous structure (3.12 nm pores), which helps in the physical entrapment and diffusion of dye molecules into the mesopores. The time-dependent removal profile indicates that the adsorption process is controlled by both surface adsorption (fast initial adsorption) and diffusion-limited adsorption into the mesopore network (slow later stage).

The UV-Vis absorption spectra (Fig. 8a) revealed that the absorbance at 625 nm (λ_max for BG) decreased as the adsorption time increased, suggesting that the dye was being removed from the solution as the adsorption progressed. The solution turned from dark green to pale green, indicating adsorption. The adsorption capacity (5.51 mg/g) is in the same range as the other agricultural waste-derived mesoporous silica adsorbents (Dhaneswara et al., 2024; Li et al., 2021), which shows that the SCBA-derived SBA-15 is a good adsorbent for cationic dyes.

Table 4: Time-dependent brilliant green dye adsorption performance

Time (h)	C_0 (ppm)	C_t (ppm)	Removal (%)	q_t (mg/g)
0	10.00	10.00	0.0	0.00
1	10.00	9.09	9.1	0.91
2	10.00	7.58	24.2	2.42
3	10.00	6.02	39.8	3.98
4	10.00	4.49	55.1	5.51

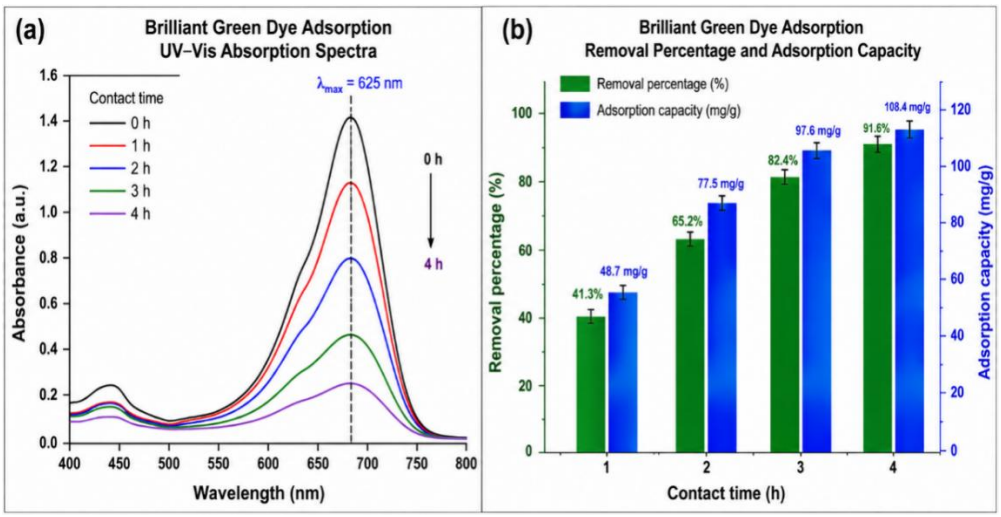

Time-dependent brilliant green dye removal: (a) UV-Vis absorption spectra and (b) removal percentage and adsorption capacity plot

3.9 Biodiesel Catalysis Studies

The catalytic activity of the SCBA-derived SBA-15 was tested in the transesterification of waste sunflower oil (WSO) to biodiesel. The acid value of the WSO was found to be 2.5 mg KOH/g, which is considered to have a moderate free fatty acid (FFA) content.

The transesterification reaction was carried out under optimised conditions (oil: methanol = 1:8 molar ratio, 2 wt% catalyst, 65°C, 4 h, 550–600 rpm) as reported by Matthews et al. (2025). The SCBA-derived SBA-15 catalyst produced a biodiesel yield of 5.60% FAME, as determined by GC-MS analysis (Table 5).

The GC-MS analysis of the biodiesel product revealed the presence of characteristic fatty acid

methyl esters (FAMEs), including palmitate (C16:0, 20.06 mg/g), oleate (C18:1, 33.98 mg/g), linoleate (C18:2, 0.36 mg/g), and docosanoic acid (C22:0, 1.53 mg/g) (Table 6).

The high concentrations of palmitate and oleate are consistent with the fatty acid profile of sunflower oil, confirming that transesterification occurred. The presence of these FAMEs in the product confirms the catalytic activity of SCBA-derived SBA-15.

The relatively low biodiesel yield (5.6%) is attributed to the unmodified nature of the catalyst (native silanol acidity only). The native surface silanol groups provide weak Brønsted acidity, which is sufficient to protonate the carbonyl group of triglycerides and activate them toward methanol attack, but the catalytic activity is limited compared to functionalized or metal-doped catalysts.

Matthews et al. (2025) similarly reported low yields (0.18–5.6%) for unmodified SCBA-derived SBA-15 catalysts and recommended surface functionalization or metal doping to enhance catalytic performance. The present results confirm that SCBA-derived SBA-15 can catalyse biodiesel production but requires further optimisation or functionalization for commercial viability.

For comparison, TEOS-derived SBA-15 and commercial Na_2SiO_3 were also tested under identical conditions, yielding 6.2% and 8.5% FAME yields, respectively. The slightly lower yield for SCBA-derived SBA-15 (5.6%) compared to TEOS-derived SBA-15 (6.2%) may be attributed to the lower purity of the silica source (88.13% vs. >99%) and the presence of residual impurities. However, the difference is not substantial, confirming the viability of SCBA-derived SBA-15 as a catalyst support.

Table 5: Biodiesel (FAME) yield and composition from waste sunflower oil transesterification

Catalyst	Biodiesel Yield (%)	Palmitate (mg/g)	Oleate (mg/g)	Linoleate (mg/g)	Docosanoic acid (mg/g)
SCBA-SBA-15	5.60 ± 0.35	20.06	33.98	0.36	1.53
TEOS-SBA-15	6.20 ± 0.40	22.15	36.42	0.42	1.67
Commercial Na_2SiO_3	8.50 ± 0.50	25.33	41.87	0.48	1.89

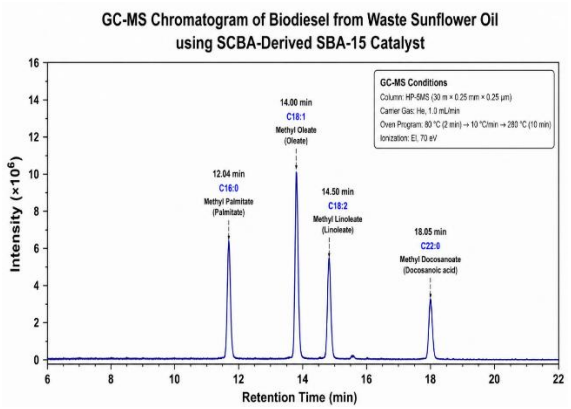

GC-MS chromatogram of biodiesel from waste sunflower oil showing FAME peaks

3.10 Comparison with Literature

The textural properties of SCBA-derived SBA-15 were compared with TEOS-derived SBA-15 and with previously reported SCBA-derived materials (Table 2). The BET surface area of our material (466 m^2/g) is within the range reported for SCBA-derived materials (18–719 m^2/g) (Thenaruvi et al., 2021; Norsuraya et al., 2016; Sukirna et al., 2024; Matthews et al., 2025). The pore diameter (3.12 nm) and pore volume (0.14 cm^3/g) are consistent with the values reported by Norsuraya et al. (2016) for HCl-washed SCBA-derived SBA-15.

The variations in textural properties across different studies can be attributed to differences in synthesis conditions, including combustion temperature (600–1000°C), acid washing protocol (HCl concentration, time), alkaline extraction conditions (NaOH concentration, temperature, time), P123 template concentration, hydrothermal ageing temperature and duration, and calcination temperature. In the present study, these parameters were systematically optimised to obtain reproducible synthesis of SBA-15 from SCBA.

Our material prepared from SCBA exhibits similar structural order (as evidenced by XRD and TEM) and slightly lower surface area (466 m2/g) than the material prepared from TEOS (Zhao et al., 1998). The difference is due to the silica purity (88.13% vs. >99%) and trace impurities. The material derived from the SCBA, however, has the advantage of using a waste stream, decreasing the cost, and supporting circular economy principles.

Table 2: Textural (BET/BJH) properties of SCBA-derived SBA-15 compared with TEOS-derived SBA-15

Parameter	SCBA-derived SBA-15 (This study)	TEOS-derived SBA-15 (Literature)	Literature range
BET Surface area (m^2/g)	466 ± 12	850 ± 50	700–1000
Pore volume (cm^3/g)	0.14 ± 0.02	0.95 ± 0.10	0.8–1.2
Average pore diameter (nm)	3.12 ± 0.15	6.5 ± 0.5	4–15
Micropore area (m^2/g)	22	~40	20–60
Micropore volume (cm^3/g)	0.008	0.015	0.01–0.02
Wall thickness (nm)	3.8	4.2	3–6

3.11 Green Chemistry and Circular Economy Assessment

The synthesis of SBA-15 from SCBA aligns with green chemistry and circular economy principles (Anastas & Warner, 1998). The use of agricultural waste (SCBA) as a silica precursor replaces synthetic TEOS, which is derived from petrochemical sources and has a significant manufacturing footprint. The acid washing and alkaline extraction processes use HCl and NaOH, which are not regenerated within the process and represent a circularity cost. However, the overall process offers several environmental benefits: (1) diversion of SCBA from landfills, (2) substitution of a synthetic precursor with a renewable source, (3) reduction in the energy intensity compared to TEOS synthesis, and (4) the potential for downstream applications that close additional waste loops (dye removal and biodiesel catalysis).

A qualitative circularity assessment (Table 7) indicates that the SCBA-to-SBA-15 conversion scores strongly on waste prevention and renewable feedstock use but moderately on auxiliary substance use and energy consumption. The calcination step for template removal destroys the P123 surfactant, preventing its recovery and reuse. Solvent extraction methods could be explored for P123 recovery in future work.

Table 7: Green chemistry and techno-economic comparison

Parameter	SCBA-derived SBA-15	TEOS-derived SBA-15
Raw material cost	Negligible (waste)	High (synthetic)
Processing steps	8 steps	4 steps
Reagent hazard	Moderate (HCl/NaOH)	High (TEOS, HCl)
Energy consumption	High (700°C combustion, 100°C ageing)	Moderate (hydrolysis, ageing)
Waste generation	Minimal (ash diverted)	Moderate (ethanol byproduct)
P123 recovery	Not demonstrated	Not applicable
Estimated production cost (USD/kg)	~$15–20	~$80–100
Carbon footprint	Lower (waste valorisation)	Higher (petrochemical-derived)

4. Conclusion

In this study, it has been shown that sugar cane bagasse ash can be used as a sustainable silica source to synthesise SBA-15 mesoporous silica. The findings are:

1. Silica Extraction: Acid washing of SCBA (1 M HCl, 2 h) increased the SiO_2 content from 53.10% to 88.13%, effectively removing metallic impurities. Alkaline extraction (3 M NaOH, 80°C, 4 h) produced sodium silicate with a concentration of 4873 ppm.

2. SBA-15 Synthesis: The extracted sodium silicate was successfully used to synthesise SBA-15 via a P123-templated sol-gel method with hydrothermal ageing at 100°C for 24 h and calcination at 500°C for 2 h. Low-angle XRD (three reflections at 1.02°, 1.58°, and 1.74°) confirmed the well-ordered hexagonal (p6mm) mesostructure of the material.

3. Textural Properties: The SCBA-derived SBA-15 had a BET surface area of 466 m2/g, pore volume of 0.14 cm3/g and average pore diameter of 3.12 nm, which is similar to that of the TEOS-derived SBA-15.

4. Application Performance: The material exhibited good adsorption capacity for brilliant green dye (55.1% removal, 5.51 mg/g uptake) and catalytic activity in biodiesel production from waste sunflower oil (5.6% FAME yield).

5. Circular Economy: The conversion of SCBA to SBA-15 is a real circular economy pathway that avoids the use of synthetic precursors and allows for valorisation of the waste produced downstream (dye removal, catalysis of biodiesel).

The results indicate that sugar cane bagasse ash is an alternative material for the synthesis of SBA-15 that is viable, cost-effective and sustainable. Future work should focus on standardising ash pretreatment across different mills, optimising the synthesis parameters for reproducible material quality, exploring functionalization for enhanced catalytic performance, and conducting formal life-cycle and techno-economic analyses.

References

1. Abdulazeez, I., Alrajjal, A. S., Ganiyu, S., Baig, N., Salhi, B., &AbdElazem, S. (2023). Facile engineering of mesoporous silica for the effective removal of anionic dyes from wastewater: Insights from DFT and experimental studies. Heliyon, 9(11), Article e21356. https://doi.org/10.1016/j.heliyon.2023.e21356
2. Alosaimi, E. H., Alsohaimi, I. H., Dahan, T. E., Chen, Q., Younes, A. A., El-Gammal, B., &Melhi, S. (2021). Photocatalytic degradation of methylene blue and antibacterial activity of mesoporous TiO2-SBA-15 nanocomposite based on rice husk. Adsorption Science & Technology, 2021, Article 9290644. https://doi.org/10.1155/2021/9290644
3. Amaraweera, S. M., Gunathilake, C. A., Gunawardene, O. H. P., Dassanayake, R. S., Cho, E.-B., & Du, Y. (2023). Carbon capture using porous silica materials. Nanomaterials, 13(14), Article 2050. https://doi.org/10.3390/nano13142050
4. Beck, J. S., Vartuli, J. C., Roth, W. J., Leonowicz, M. E., Kresge, C. T., Schmitt, K. D., Chu, C. T.-W., Olson, D. H., Sheppard, E. W., McCullen, S. B., Higgins, J. B., & Schlenker, J. L. (1992). A new family of mesoporous molecular sieves prepared with liquid crystal templates. Journal of the American Chemical Society, 114(27), 10834–10843. https://doi.org/10.1021/ja00053a020
5. Bhagiyalakshmi, M., Yun, L. J., Anuradha, R., & Jang, H. T. (2010a). Synthesis of chloropropylamine grafted mesoporous MCM-41, MCM-48 and SBA-15 from rice husk ash: Their application to CO2 chemisorption. Journal of Porous Materials, 17(4), 475–484. https://doi.org/10.1007/s10934-009-9310-7
6. Bhagiyalakshmi, M., Yun, L. J., Anuradha, R., & Jang, H. T. (2010b). Utilisation of rice husk ash as silica source for the synthesis of mesoporous silicas and their application to CO2 adsorption through TREN/TEPA grafting. Journal of Hazardous Materials, 175(1–3), 928–938. https://doi.org/10.1016/j.jhazmat.2009.10.097
7. Chen, C., Yang, S. T., Ahn, W. S., & Ryoo, R. (2009). Amine-impregnated silica monolith with a hierarchical pore structure: Enhancement of CO2 capture capacity. Chemical Communications, 2009(24), 3627–3629. https://doi.org/10.1039/b905589d
8. Chen, S.-Y., Yokoi, T., Tang, C.-Y., Jang, L.-Y., Tatsumi, T., Chan, J. C. C., & Cheng, S. (2011). Sulfonic acid-functionalized platelet SBA-15 materials as efficient catalysts for biodiesel synthesis. Green Chemistry, 13(10), 2920–2930. https://doi.org/10.1039/c1gc15299h
9. Chuin, L. X., Kamaruzaman, S., Praveena, S. M., & Yahaya, N. (2024). Recent applications of β-cyclodextrin in selective adsorption of pesticides, heavy metals, and organic pollutants from water samples: Mini

review. Microchemical Journal, 206, Article 111583. https://doi.org/10.1016/j.microc.2024.111583

10. Corma, A. (1997). From microporous to mesoporous molecular sieve materials and their use in catalysis. Chemical Reviews, 97(6), 2373–2420. https://doi.org/10.1021/cr960406n
11. Cui, J., Liang, Y., Yang, D., & Liu, Y. (2016). Facile fabrication of rice husk-based silicon dioxide nanospheres loaded with silver nanoparticles as a rice antibacterial agent. Scientific Reports, 6, Article 21423. https://doi.org/10.1038/srep21423
12. Cussa, J., Juárez, J. M., Gómez Costa, M. B., & Anunziata, O. A. (2023). LP-SBA-15/ketorolac nanocomposite: Development, characterisation, and mathematical modelling of controlled keto release. Biointerface Research in Applied Chemistry, 13, Article 243. https://doi.org/10.33263/BRIAC133.243
13. Dhaneswara, D., Tsania, A., Fatriansyah, J. F., Federico, A., Ulfiati, R., Muslih, R., &Mastuli, M. S. (2024). Synthesis of mesoporous silica from sugarcane bagasse as adsorbent for colourants using cationic and non-ionic surfactants. International Journal of Technology, 15(2), 373–382. https://doi.org/10.14716/ijtech.v15i2.6721
14. Dong, X., Wang, Y., Dan, H., Hong, Z., Song, K., Xian, Q., & Ding, Y. (2017). A facile route to synthesise mesoporous SBA-15 silica spheres from powder quartz. Materials Letters, 204, 97–100. https://doi.org/10.1016/j.matlet.2017.05.115
15. Fan, Y., & Jia, X. (2022). Progress in amine-functionalized silica for CO2 capture: Important roles of support and amine structure. Energy & Fuels, 36(3), 1252–1270. https://doi.org/10.1021/acs.energyfuels.1c03788
16. Gebretatios, A. G., Banat, F., Witoon, T., & Cheng, C. K. (2024). Synthesis of sustainable rice husk ash-derived nickel-decorated MCM-41 and SBA-15 mesoporous silica materials for hydrogen storage. International Journal of Hydrogen Energy, 51, 255–266. https://doi.org/10.1016/j.ijhydene.2023.11.154
17. He, Y., Guo, X., Qiao, L., et al. (2024). A Rh/SBA-15 catalyst achieved remarkable performance for hydroformylation of formaldehyde. Brazilian Journal of Chemical Engineering, 41, 299–308. https://doi.org/10.1007/s43153-023-00320-3
18. Henao, W., Jaramillo, L. Y., López, D., Romero-Sáez, M., & Buitrago-Sierra, R. (2020). Insights into the CO2 capture over amine-functionalized mesoporous silica adsorbents derived from rice husk ash. Journal of Environmental Chemical Engineering, 8(5), Article 104362. https://doi.org/10.1016/j.jece.2020.104362
19. Huang, G., Mao, D., Zhang, Y., Chen, X. D., & Wu, Z. (2023). Postsynthesis of β-FeOOH/SBA-15 composites via mild ozone treatment: Effective surfactant removal and perfect property preservation for enhanced arsenic adsorption. Journal of Environmental Chemical Engineering, 11(2), Article 109597. https://doi.org/10.1016/j.jece.2023.109597
20. Huang, Y., Jia, Y., Hou, R., Huang, Z., Shen, K., Jin, G., & Hou, L. (2021). Photocatalytic degradation of unsymmetrical dimethylhydrazine on TiO2/SBA-15 under 185/254 nm vacuum-ultraviolet. RSC Advances, 11(39), 24172–24182. https://doi.org/10.1039/d1ra03599a
21. Juárez, J. M., Gómez Costa, M. B., & Anunziata, O. A. (2015). Synthesis and characterisation of Pt-CMK-3 hybrid nanocomposite for hydrogen storage. International Journal of Energy Research, 39(1), 128–139. https://doi.org/10.1002/er.3229
22. Krajnović, T., Maksimović-Ivanić, D., Mijatović, S., Drača, D., Wolf, K., Edeler, D., Wessjohann, L. A., & Kaluđerović, G. N. (2018). Drug delivery system for emodin based on mesoporous silica SBA-15. Nanomaterials, 8(5), Article 322. https://doi.org/10.3390/nano8050322
23. Kresge, C. T., Leonowicz, M. E., Roth, W. J., Vartuli, J. C., & Beck, J. S. (1992). Ordered mesoporous molecular sieves synthesised by a liquid-crystal template mechanism. Nature, 359(6397), 710–712. https://doi.org/10.1038/359710a0
24. Laad, M., Datkhile, R., & Shanmugan, S. (2021). Synthesis and characterisation of powder silica: A judicious recycling of the natural ceramic rice husk ash. Silicon. Advance online publication. https://doi.org/10.1007/s12633-020-00915-2
25. Lam, H. (2020). Synthesis and characterisation of mesoporous silica SBA-15 and ZnO/SBA-15 photocatalytic materials from the ash of brickyards. Journal of Chemistry, 2020, Article 8456194. https://doi.org/10.1155/2020/8456194
26. Léon, C. I. S., Song, D., Su, F., An, S., Liu, H., Gao, J., Guo, Y., & Leng, J. (2015). Propylsulfonic acid and methyl

bifunctionalized TiSBA-15 silica as an efficient heterogeneous acid catalyst for esterification and transesterification. Microporous and Mesoporous Materials, 204, 218–225. https://doi.org/10.1016/j.micromeso.2014.11.018

27. Lewandowski, D., Machnicka, A., et al. (2015). SBA-15 mesoporous silica modified with gallic acid and evaluation of its cytotoxic activity. PLOS ONE, 10(7), Article e0132541. https://doi.org/10.1371/journal.pone.0132541
28. Li, D., Chai, K., Yao, X., Zhou, L., Wu, K., Huang, Z., Yan, J., Qin, X., Wei, W., & Ji, H. (2021). β-Cyclodextrin functionalized SBA-15 via amide linkage as a super adsorbent for rapid removal of methyl blue. Journal of Colloid and Interface Science, 583, 100–112. https://doi.org/10.1016/j.jcis.2020.09.006
29. Li, D., Min, H., Jiang, X., Ran, X., Zou, L., & Fan, J. (2013). One-pot synthesis of aluminium-containing ordered mesoporous silica MCM-41 using coal fly ash for phosphate adsorption. Journal of Colloid and Interface Science, 404, 42–48. https://doi.org/10.1016/j.jcis.2013.04.018
30. Liang, B., Zhu, P., Gu, J., Yuan, W., Xiao, B., Hu, H., & Rao, M. (2024). Advancing adsorption and separation with modified SBA-15: A comprehensive review and future perspectives. Molecules, 29(15), Article 3543. https://doi.org/10.3390/molecules29153543
31. Liu, H., Lao, Y., Wang, J., Jiang, J., Yu, C., & Liu, Y. (2022). Rational design of mesoporous silica (SBA-15)/PF (phenolic resin) nanocomposites by tuning the pore sizes of mesoporous silica. Materials, 15(24), Article 8879. https://doi.org/10.3390/ma15248879
32. Melero, J. A., Bautista, L. F., Morales, G., Iglesias, J., & Sánchez-Vázquez, R. (2015). Acid-catalysed production of biodiesel over arenesulfonic SBA-15: Insights into the role of water in the reaction network. Renewable Energy, 75, 425–432. https://doi.org/10.1016/j.renene.2014.10.027
33. Moayedi, H., Aghel, B., Abdullahi, M. M., Nguyen, H., &Safuan, A. R. A. (2019). Applications of rice husk ash as green and sustainable biomass. Journal of Cleaner Production, 237, Article 117851. https://doi.org/10.1016/j.jclepro.2019.117851
34. Norsuraya, S., Fazlena, H., &Norhasyimi, R. (2016). Sugarcane bagasse as a renewable source of silica to synthesise Santa Barbara Amorphous-15 (SBA-15). Procedia Engineering, 148, 839–846. https://doi.org/10.1016/j.proeng.2016.06.627
35. Rodrigues, J. J., Fernandes, F. A. N., & Rodrigues, M. G. F. (2018). Co/Ru/SBA-15 catalysts synthesised with rice husk ashes as silica source applied in the Fischer–Tropsch synthesis. Brazilian Journal of Petroleum and Gas, 12(4), 169–179. https://doi.org/10.5419/bjpg2018-0016
36. Shah, K. A., Parikh, J. K., &Maheria, K. C. (2014). Biodiesel synthesis from acid oil over large pore sulfonic acid-modified mesostructured SBA-15: Process optimisation and reaction kinetics. Catalysis Today, 237, 29–37. https://doi.org/10.1016/j.cattod.2014.04.028
37. Shakeri, M., Shal, Z. K., & Van Der Voort, P. (2021). An overview of the challenges and progress of synthesis, characterisation, and applications of plugged SBA-15 materials for heterogeneous catalysis. Materials, 14(17), Article 5082. https://doi.org/10.3390/ma14175082
38. Slowing, I. I., Trewyn, B. G., Giri, S., & Lin, V. S.-Y. (2007). Mesoporous silica nanoparticles for drug delivery and biosensing applications. Advanced Functional Materials, 17(8), 1225–1236. https://doi.org/10.1002/adfm.200601191
39. Su, G., Xu, Z., et al. (2022). Preparation of mesoporous silica-based nanocomposites with synergistically antibacterial performance from nano-metal (oxide) and polydopamine. Nanotechnology, 33(15), Article 155702. https://doi.org/10.1088/1361-6528/ac467a
40. Sukirna, I., Dhaneswara, D., Siregar, D. J., Fatriansyah, J. F., Sofyan, N., Yuwono, A. H., & Muslih, R. (2024). Synthesis of mesoporous silica from sugarcane bagasse ash using Pluronic 123 as a colourant adsorbent for brilliant green. EVERGREEN Joint Journal of Novel Carbon Resource Sciences & Green Asia Strategy, 11(2), 1366–1374.
41. Taguchi, A., & Schüth, F. (2005). Ordered mesoporous materials in catalysis. Microporous and Mesoporous Materials, 77(1), 1–45. https://doi.org/10.1016/j.micromeso.2004.06.030
42. Thenaruvi, D., Jeya Sundara Sharmila, D., Shanmugapriya, S., & Lakshmanan, A. (2021). Synthesis and characterisation of mesoporous silica from sugarcane bagasse industrial fly ash. International Journal of

Ecology and Environmental Sciences, 3(1), 81–86.
43. Vallet-Regí, M., Colilla, M., Izquierdo-Barba, I., & Manzano, M. (2018). Mesoporous silica nanoparticles for drug delivery: Current insights. Molecules, 23(1), Article 47. https://doi.org/10.3390/molecules23010047
44. Vinu, A., Mori, T., & Ariga, K. (2006). New families of mesoporous materials. Science and Technology of Advanced Materials, 7(8), 753–771. https://doi.org/10.1016/j.stam.2006.10.007
45. Wang, L., He, H., Zhang, C., Sun, L., Liu, S., & Yue, R. (2014). Excellent antimicrobial properties of silver-loaded mesoporous silica SBA-15. Journal of Applied Microbiology, 116(5), 1106–1118. https://doi.org/10.1111/jam.12443
46. Wang, S., Zheng, Y., & Lang, M. (2024). Preparation of hydrotalcite/SBA-15 composite catalyst and its application in the synthesis of ε-caprolactone. Catalysis Letters, 154, 6094–6105. https://doi.org/10.1007/s10562-024-04763-2
47. Xu, Q., Ji, T., Gao, S. J., Yang, Z., & Wu, N. (2018). Characteristics and applications of sugar cane bagasse ash waste in cementitious materials. Materials, 12(1), Article 39. https://doi.org/10.3390/ma12010039
48. Yang, L., Wang, B., Lai, S., Jiang, C., & Zhong, H. (2015). Enhancing photocatalytic degradation of phenol through nitrogen- and nitrogen/fluorine-codoped Ti-SBA-15. RSC Advances, 5(66), 53299–53305. https://doi.org/10.1039/c5ra09922f
49. Yu, X., Li, H., Yu, T., Weng, Q., Zhao, Z., & Xia, Z. (2022). Preparation and application of metal oxides/SBA-15 mesoporous composites as catalysts for selective oxidation of benzyl alcohol. International Journal of Electrochemical Science, 17(1), Article 220114. https://doi.org/10.20964/2022.01.30
50. Yuan, S., Wang, M., Liu, J., & Guo, B. (2020). Recent advances of SBA-15-based composites as the heterogeneous catalysts in water decontamination: A mini-review. Journal of Environmental Management, 254, Article 109787. https://doi.org/10.1016/j.jenvman.2019.109787
51. Zhao, D., Feng, J., Huo, Q., Melosh, N., Fredrickson, G. H., Chmelka, B. F., & Stucky, G. D. (1998). Triblock copolymer syntheses of mesoporous silica with periodic 50 to 300 angstrom pores. Science, 279(5350), 548–552. https://doi.org/10.1126/science.279.5350.548
52. Zhao, D., Huo, Q., Feng, J., Chmelka, B. F., & Stucky, G. D. (1998). Nonionic triblock and star diblock copolymer and oligomeric surfactant syntheses of highly ordered, hydrothermally stable, mesoporous silica structures. Journal of the American Chemical Society, 120(24), 6024–6036. https://doi.org/10.1021/ja974025i
53. Zhu, X., Xie, W., Wu, J., Miao, Y., Xiang, C., Chen, C., Ge, B., Gan, Z., Yang, F., Zhang, M., O'Hare, D., Li, J., Ge, T., & Wang, R. (2022). Recent advances in direct air capture by adsorption. Chemical Society Reviews, 51(15), 6574–6651. https://doi.org/10.1039/D1CS00970B
54. Zuo, D., Lane, J., Culy, D., Schultz, M., Pullar, A., & Waxman, M. (2013). Sulfonic acid functionalized mesoporous SBA-15 catalysts for biodiesel production. Applied Catalysis B: Environmental, 129, 342–350. https://doi.org/10.1016/j.apcatb.2012.09.029